X-ray-absorption studies of zirconia polymorphs. II. Effect of Y_2O_3 dopant on ZrO_2 structure

Ping Li and I-Wei Chen
Department of Materials Science and Engineering, University of Michigan, Ann Arbor, Michigan 48109-2136

James E. Penner-Hahn
Department of Chemistry, University of Michigan, Ann Arbor, Michigan 48109-1055
(Received 10 March 1993; revised manuscript received 28 May 1993)

Extended x-ray-absorption fine structure and x-ray-absorption near-edge structure spectra at both the Zr and Y K edge have been obtained at 10 K and room temperature for solid ZrO_2-Y_2O_3 solutions. Zr has very different local structures in the tetragonal and cubic solid solutions in terms of the oxygen-bond distances and coordination number. In contrast, the Y local structure is nearly the same in all of the solid solutions. Charge-compensating oxygen vacancies caused by Y doping are preferentially located next to Zr ions, leaving eightfold oxygen coordination for the Y ions. The nearest-neighbor and next-nearest-neighbor distances in these solid solutions do not follow the virtual-crystal approximation with reference to x-ray-diffraction lattice parameter. The distortion of the Zr-cation shell in cubic solid solutions is especially severe so that the long-range fluoritelike order implied by global cubic symmetry is not manifested in the local atomic environment.

I. INTRODUCTION

It is well known that zirconia can be stabilized by appropriate dopants.[1–4] Yttria-stabilized zirconia is the most studied system and the one most used in various applications ranging from oxygen sensors to structural components. ZrO_2-Y_2O_3 solid solutions contain a distribution of both Y solute cations and charge-compensating oxygen vacancies. Questions have been raised regarding the location of the vacancies with respect to the dopant and host cations. A related question concerning the distortion of the cations and anions around these vacancies is also of interest.[5–8] Charge considerations suggest that the Y cation is the most likely nearest neighbor of oxygen vacancies.[5,6] On the other hand, Y, being an oversized cation, could conceivably prefer an eightfold oxygen coordination, leaving oxygen vacancies to Zr cations.[8–11] Resolution of this issue and the related distortion question is important for understanding the phase stability and ionic conductivity of ZrO_2-Y_2O_3 solid solutions. Previous diffraction studies were unable to resolve this issue because Y and Zr, which have nearly the same scattering factors, cannot be distinguished. This deficiency, which is a general problem for diffraction studies of solid solutions, can be remedied by using a local, element-specific structural probe such as x-ray-absorption spectroscopy (XAS).

Several XAS studies have already been reported for this system.[11–18] Most of these studies were carried out in the high-Y-concentration regime and thus limited to the cubic-phase field. The disagreement among investigators of these studies has again centered on the location of the oxygen vacancies. Goldman *et al.*,[11] Tuilier *et al.*,[13] Morikawa *et al.*,[15] and Shen *et al.*[16] concluded that oxygen vacancies were associated with the aliovalent dopants. Catlow *et al.*,[12] Komyoji *et al.*,[18] and Veal *et al.*[14] thought that oxygen vacancies were removed from the stabilizing dopant and most likely incorporated into the Zr-O shell. This disagreement arises primarily because of different interpretations of the coordination number (N_{CN}) obtained from fitting the extended x-ray-absorption fine structure (EXAFS) data. This is unnecessary, however, since EXAFS coordination numbers have only low accuracy, ~20%,[19] and should not be overinterpreted.

More systematic study over a wider compositional range, and possibly including other reference zirconia compounds, is needed to reach a more definitive conclusion. This is attempted in the present work which covers both the tetragonal- and cubic-phase fields. To aid interpretation of the EXAFS and x-ray-absorption near-edge structure (XANES) data, model calculations were performed to determine the oxygen-vacancy distribution. In addition, the EXAFS distances for cation-O and cation-cation bonds in this model solid solution were compared with the predictions of the virtual-crystal approximation (VCA) using x-ray-diffraction (XRD) lattice parameters to shed light on the tetragonal and cubic structures.

II. EXPERIMENTAL PROCEDURE

A. Materials

The preparation method used for our powder samples has been described in the preceding paper (I).[4] Ultrafine ZrO_2 powders doped with 3, 6, 10, 15, and 20 mol % Y_2O_3 were prepared by coprecipitation and then calcined at 1300 °C. Phase identification and lattice parameter measurements were made by x-ray diffraction. The results of this analysis are shown in Table I. These results are consistent with the phase diagram of this system.[20] The lattice parameter increases with increasing Y_2O_3 concentration in the cubic region, and its magnitude is in

TABLE I. Phase identification of Y-stabilized zirconia samples.

Y_2O_3 concentration (mol %)	Phase	Lattice parameter (Å)
		$a=5.1060$
3	t	$c=5.1808$
6	$t+c$	5.1353
10	c	5.1486
15	c	5.1626
20	c	5.1748

good agreement with previous studies.[1,2] This indicates that the Y ions, which are larger than Zr ions, are incorporated into the zirconia lattice, causing an increase in the average unit-cell volume.

B. X-ray-absorption measurements

X-ray-absorption measurements were made at 10 K for 3 and 20 mol % Y_2O_3-ZrO_2 on Beamline 7-3 at the Stanford Synchrotron Radiation Laboratory (SSRL). Room-temperature measurements at both edges were made for 3, 6, 10, 15, and 20 mol % Y_2O_3-ZrO_2 on Beamline X10-C at the National Synchrotron Light Source (NSLS) at Brookhaven National Laboratory. The experimental procedure at SSRL was the same as described in paper I. At NSLS, a double-crystal monochromator with Si(333) crystals was employed and Ti filters with 18 paths were used as a high-pass filter to remove the fundamental ($\sim$6 keV) and pass the first harmonic ($\sim$18 keV) of the beam. The absorption spectra of pure monoclinic ZrO_2 and pure C-type Y_2O_3 were measured simultaneously as references and as energy calibration standards. The data were calibrated by assigning the highest inflection points of the Zr K edge in m-ZrO_2 as 17 998 eV and of the Y K edge in Y_2O_3 as 17 038 eV.

C. Data analysis

Analysis of the Zr K-edge data followed the procedure described in paper I. Two methods were used to determine the Y EXAFS scattering amplitude and phase functions. In the first method, these quantities were calculated theoretically using the FEFF program (version 3.0).[21] The calculation used the Y-O distance of 2.28 Å, which is representative of C-type Y_2O_3.[26] Alternatively, they could be determined empirically using the experimental EXAFS data for Y_2O_3. The fitting parameter E_0 was initially assigned as 17 055 eV and then varied so that the Y-O distance of 2.28 Å in Y_2O_3 could be reproduced. The optimum E_0 value was 17 076 eV for the first (*ab initio*) method and 17 055 eV for the second (empirical) method. These values were used in the analysis which left the bond distance R, coordination number N_{CN}, and bond dispersion σ (Debye-Waller factor) as adjustable parameters to obtain the best fit to the experimental data. Since both methods gave very similar R and N_{CN}, but *ab initio* parameters allowed determination of an absolute σ, we only report results obtained using the first method. For analysis of cation-cation scattering, FEFF was used for a Y-Zr pair (or a Zr-Zr pair) with a distance of 3.628 Å. No attempt was made to differentiate Y and Zr scatterers; both were treated as Zr since the scattering behavior of Y and Zr is nearly the same. Fourier-filtered windows used to isolate each shell are given in Table II.

III. RESULTS

A. Local environments of Zr and Y in zirconia solid solutions

Low-temperature measurements can enhance the EXAFS signal, particularly at high-k values, due to reduced thermal motion. Since no detectable phase transformation was observed on cooling to 10 K, we first focus on the low-temperature data to compare the local environments around Zr and Y ions in two representative tetragonal and cubic structures. The effect of Y concentration is dealt with in the next subsection.

1. Tetragonal zirconia (3 mol % Y_2O_3)

The EXAFS spectra shown in Figs. 1(a) and 1(b) have a good signal-to-noise ratio out to $k=17$ Å^{-1}. However, only the data below 14 Å^{-1} is usable for Y because of the presence of the Zr K edge at $k\sim14$ Å^{-1}. The Fourier transforms (FT's) of these EXAFS spectra are given in Fig. 2. The Zr-O peak has a characteristic broad, two-subshell structure,[4] while the Y-O peak is much sharper. The next-nearest neighbors (NNN's) for Zr and Y, however, are at the same distance. This indicates that Zr and

TABLE II. EXAFS results of ZrO_2-Y_2O_3 solid solutions at 10 K.[a]

		Zr K edge						Y K edge					
Composition	Bonding	ΔR_{filt} (Å)	Δk (Å^{-1})	R (Å)	N_{CN}	σ^2 (Å^2)	ρ (%)[b]	ΔR_{filt} (Å)	Δk (Å^{-1})	R (Å)	N_{CN}	σ^2 (Å^2)	ρ (%)[b]
3 mol % Y_2O_3	cation-O	1.0–2.1	3.0–13.0	2.10	4.0	0.0034	2.3	1.0–2.3	2.8–12.0	2.33	8.0	0.0077	7.8
(tetragonal)				2.33	4.0	0.0090							
	cation-cation	2.7–3.7	3.0–17.0	3.62	12.0	0.0034	0.3	2.7–3.7	2.8–12.0	3.62	12.0	0.0036	0.8
20 mol % Y_2O_3	cation-O	0.9–1.9	3.0–13.0	2.15	7.0	0.0074	2.9	1.0–2.2	2.8–12.0	2.32	8.0	0.0096	9.0
(cubic)	cation-cation	2.4–3.4	3.0–17.0	3.55	12.0	0.0090	1.4	2.5–3.7	2.8–12.0	3.62	12.0	0.0065	1.2

[a]Fixed at values shown during fitting.

[b]Relative deviation between experimental data and calculated EXAFS. $\rho=\sum(k^3\chi_{expt}-k^3\chi_{calc})^2/\sum(k^3\chi_{expt})^2$.

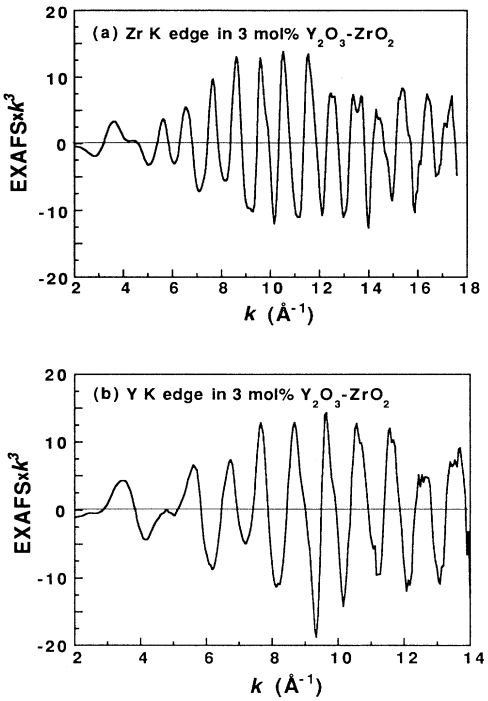

FIG. 1. EXAFS spectra of (a) Zr K edge and (b) Y K edge for t-ZrO_2 with 3 mol % Y_2O_3 at 10 K.

Y have formed a solid solution but have different nearest-neighbor (NN) structures.

The quantitative curve-fitting results are given in Table II. The Zr-O shell consists of two subshells, 2.10 and 2.33 Å, as in paper I. In contrast, a single Y-O shell is found at 2.33 Å, which is consistent with the values reported in the literature.[11,13,15,16] This distance is larger than that for Y-O in Y_2O_3 (2.28 Å) and implies, according to crystal chemistry, a higher coordination number for the Y in zirconia. Our analysis also confirms that the Zr NNN and the Y NNN shells have the same distance (3.62 Å).

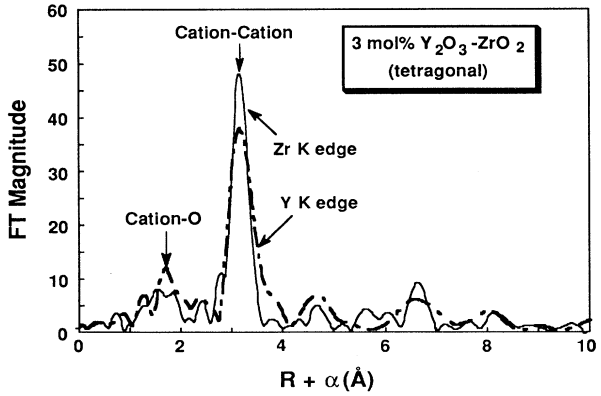

FIG. 2. Fourier transforms of Zr and Y EXAFS for t-ZrO_2 doped with 3 mol % Y_2O_3 at 10 K.

2. *Cubic zirconia (20 mol % Y_2O_3)*

The EXAFS spectra for the Zr and Y K edges shown in Figs. 3(a) and 3(b), respectively, are obviously different in their shape, amplitude, and frequency, implying different local structures. The Zr EXAFS is also different from that in Fig. 1(a), but the Y spectrum is similar in shape to that in Fig. 1(b). Thus the characteristic Zr local structure depends on lattice type, but the Y local structure does not.

The FT's shown in Fig. 4 reveal only two distinct peaks. The Y-O shell has a lower amplitude than the Zr-O shell, while the Y-cation shell has a higher amplitude than the Zr-cation shell. Peaks in cubic zirconia generally have lower amplitudes than the corresponding peaks in tetragonal zirconia (Fig. 4 vs Fig. 2). A better appreciation of the differences in the second shells of the two phases can be obtained by isolating the second-shell contributions through Fourier filtering. These data, back transformed to k space, are shown in Fig. 5. The Zr-cation EXAFS frequency is lower in cubic zirconia than in tetragonal zirconia, implying a shorter distance in the cubic structure. In contrast, the Y-cation EXAFS frequency is the same in cubic and tetragonal zirconia, implying the same distance. Also, the cubic Zr-cation spectrum is by far the weakest of the spectra in Fig. 5. This implies a considerable disorder in the cubic Zr-cation shell.

The quantitative curve-fitting results are summarized in Table II. The Zr-O shell fits a single shell at 2.15 Å×7, unlike the two subshells seen before. The Zr-cation distance of 3.55 Å is shorter than the correspond-

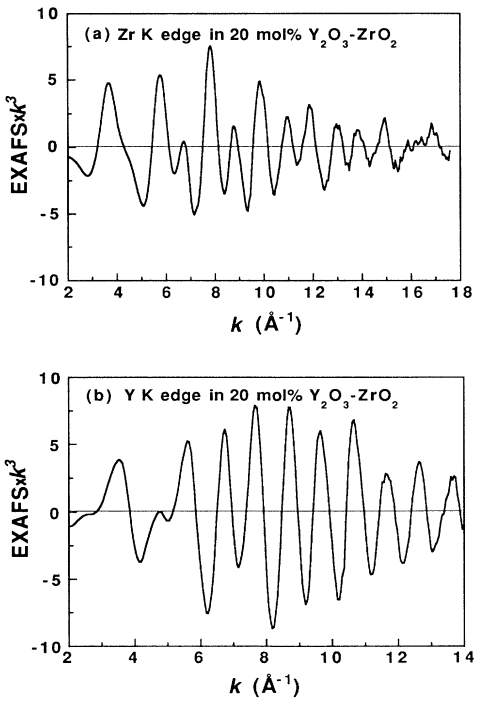

FIG. 3. EXAFS spectra of (a) Zr K edge and (b) Y K edge for c-ZrO_2 doped with 20 mol % Y_2O_3 at 10 K.

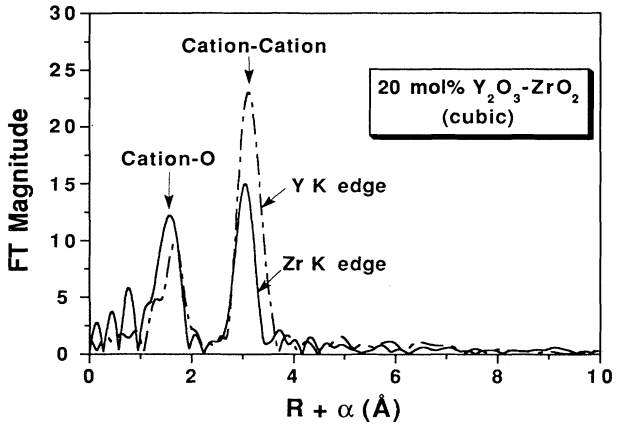

FIG. 4. Fourier transforms of Zr and Y EXAFS for c-ZrO_2 doped with 20 mol % Y_2O_3 at 10 K.

ing distance (3.62 Å) in tetragonal zirconia.[4] In contrast, the Y local environment is not sensitive to the host-crystal structure in either R (2.33 Å for Y-O and 3.62 Å for Y-cation) or N_{CN} (8 and 12, respectively). Note that the Y-cation distance coincides with the Zr-Zr distance in t-ZrO_2.

The values for the Debye-Waller factor in Table II indicate that the distortion generally increases from tetragonal to cubic zirconia. However, the distortion of the Zr-centered cation network in cubic zirconia is especially large. These observations are consistent with the amplitude variation noted in Fig. 5. An important consequence of the large disorder in the Zr-cation shell is that

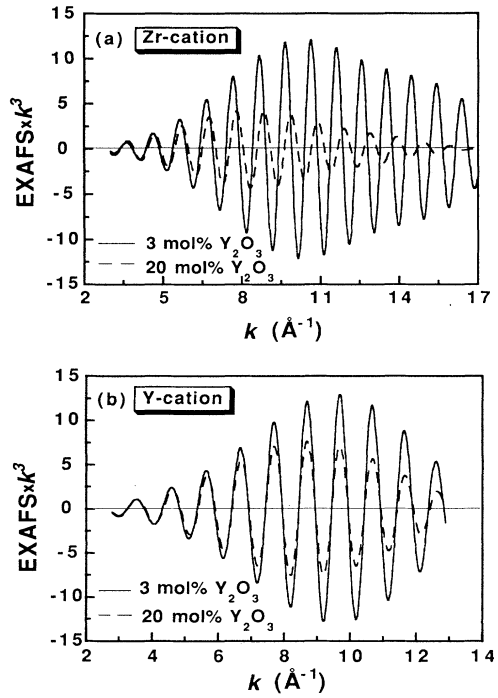

FIG. 5. EXAFS spectra for (a) Zr-cation shell and (b) Y-cation shell in both t- and c-ZrO_2 at 10 K.

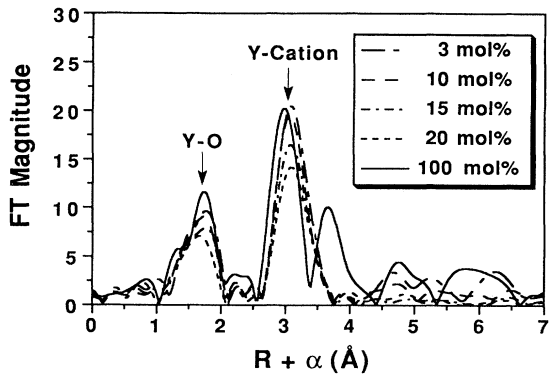

FIG. 6. Fourier transforms of Y EXAFS for yttria and Y-doped zirconia at room temperature.

EXAFS-derived distances are likely underestimated because of the possibility of a non-Gaussian dispersion in the bond distance.[19] Therefore the observed decrease in Zr-cation distance with increasing Y_2O_3 content may not represent a true contraction.[4]

B. Dependence of zirconia structure on Y_2O_3 concentration

To further elucidate the relationship between the tetragonal and cubic structures and the compositional dependence, EXAFS and XANES spectra were compared over a range of Y_2O_3 compositions (3, 6, 10, 15, and 20 mol %). Although these EXAFS data were measured at room temperature, the essential features which distinguish the spectra are still manifest despite the loss of some details due to increased thermal disorder. No difference was found between XANES data of 10 K and room temperature.

1. XAS spectra at the Y K edge

All the FT's for zirconia solid solutions shown in Fig. 6 have similar distances for both the Y-O shell and the Y-

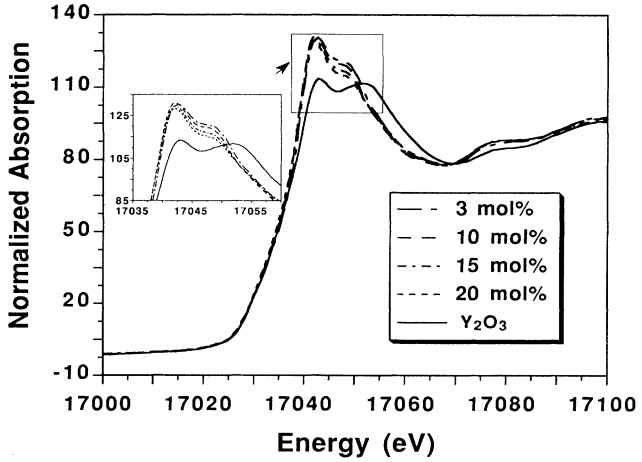

FIG. 7. XANES spectra of Y K edge for yttria and Y-doped zirconia.

cation shell. The amplitude, however, decreases continuously with increasing Y concentration. Quantitative analysis confirms the same bond distance (2.33 Å) for the Y-O shell as for all compositions. Likewise, a similar distance (~3.62 Å) is found for all of the Y-cation shells. Aside from the increase in disorder (σ) with composition, the local environment of Y ions in zirconia is insensitive to the composition or the phase. It is, however, obviously different from that in Y_2O_3 which has a totally distinct FT (Fig. 6).

The XANES spectra shown in Fig. 7 reveal several features. First, similar near-edge structures are observed in all the Y-stabilized zirconia, indicating similar local structures in tetragonal (3Y) and cubic (10Y, 15Y, and 20Y) forms. These structures are different from that in Y_2O_3. Second, the slopes are steeper (i.e., the edge width is narrower) and the amplitudes are higher in the zirconia solid solutions relative to Y_2O_3. These features are usually associated with a more ionic nature of the probe atoms, which would be consistent with a higher N_{CN} and a longer Y-O distance in the zirconia solid solutions. Third, a splitting of the main peak in pure Y_2O_3, which has been previously reported in the literature, is confirmed by our data. Indeed, we see a slightly larger energy separation [9 eV compared with 7 eV (Refs. 22 and 23)]. A similar splitting, but with a smaller separation (~6.5 eV), is observed in all the zirconia solid solutions.

2. *XAS spectra at Zr K edge*

Three features of the FT's for Zr EXAFS (Fig. 8) are immediately noticeable. First, the two-shell structure of the Zr-O peak observed at 10 K (Fig. 2) for the 3-mol % Y_2O_3 sample is not evident at room temperature. Second, the amplitude of the Zr-O shell increases and the amplitude of the Zr-cation shell decreases with increasing Y_2O_3 concentration. Third, the Zr-cation distance seems to contract with increasing Y concentration. Quantitative curve-fitting results (Table III) are consistent with these qualitative observations. For 3 mol % Y_2O_3-stabilized tetragonal zirconia, the best fit to the Zr-O shell gives fourfold coordination with a Zr-O distance of 2.10 Å. Thus only the inner Zr-O subshell (Table II) is

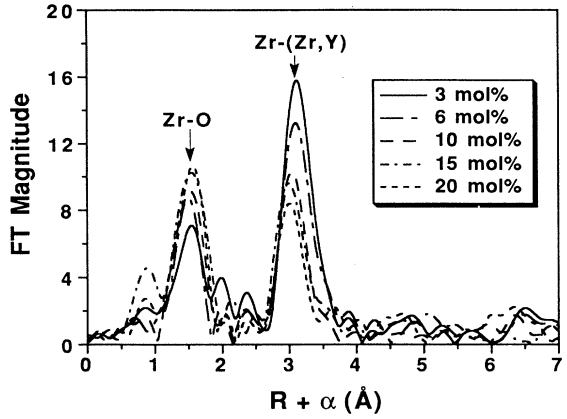

FIG. 8. Fourier transforms of Zr EXAFS for Y-doped zirconia at room temperature.

observed at room temperature. This accounts for the surprisingly low apparent coordination number and bond length (Table III). The outer subshell disappears because of increased disorder in these longer, looser Zr-O bonds. With only the first subshell remaining, the first peak in the tetragonal spectrum in Fig. 8 appears weak. In the cubic phase field (10–20 mol % Y_2O_3), a sevenfold-coordinated Zr-O shell with a bond length of 2.15 Å is found, and the Debye-Waller factor actually decreases with increasing Y concentration. This accounts for the increasing amplitude of the first FT peak with increasing Y_2O_3 concentration in this field (Fig. 8). We also confirm that the apparent Zr-cation distance continuously decreases from 3.62 to 3.55 Å, and the Debye-Waller factor increases from 3 to 20 mol % Y_2O_3.

The XANES spectra at the Zr K edge are shown in Fig. 9. The first derivatives of these spectra are shown in Fig. 10 in order to highlight some of the subtle features. Three features which change systematically with Y concentration are noted here. First, peak A, a small shoulder on the edge rising in Fig. 9 at about 6 eV beyond the Zr K-edge threshold, decreases with increasing Y_2O_3 concentration. This is clearer in the first derivative plot (Fig. 10) where the feature is labeled A'. As suggested before,[4] this feature can be attributed to a $1s \rightarrow 4d$ transition

TABLE III. EXAFS results of Y-stabilized zirconia at various compositions (room temperature).

Y_2O_3 concentration (mol %)	Bonding	Zr K edge R (Å)	Zr K edge N_{CN}[a]	Zr K edge σ^2 (Å^2)	Y K edge R (Å)	Y K edge N_{CN}[a]	Y K edge σ^2 (Å^2)
3	cation-oxygen	2.10	4.0	0.0048	2.33	8.0	0.0080
	cation-cation	3.62	12.0	0.0076	3.62	12.0	0.0069
6	cation-oxygen	2.13	5.0	0.0064	2.33	8.0	0.0088
	cation-cation	3.62	12.0	0.0086	3.62	12.0	0.0069
10	cation-oxygen	2.15	7.0	0.0094	2.33	8.0	0.0088
	cation-cation	3.58	12.0	0.0108	3.62	12.0	0.0074
15	cation-oxygen	2.15	7.0	0.0088	2.33	8.0	0.0094
	cation-cation	3.56	12.0	0.0112	3.62	12.0	0.0083
20	cation-oxygen	2.15	7.0	0.0085	2.32	8.0	0.0108
	cation-cation	3.55	12.0	0.0125	3.62	12.0	0.0090

[a]Fixed at values shown during fitting (see text).

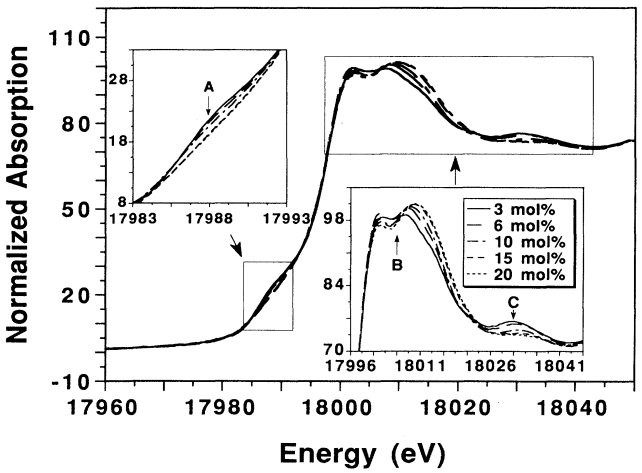

FIG. 9. XANES spectra of Zr K edge for Y-doped zirconia.

which is enhanced by tetrahedral geometry that allows more d-p mixing than in sevenfold coordination. This is consistent with the EXAFS results which suggest that Zr-O bonding changes progressively from 3 mol % Y_2O_3 (two sets of tetrahedral coordination) to 15 and 20 mol % Y_2O_3 (sevenfold coordination). (A similar decrease in this feature with increasing dopant concentration was previously observed in rare-earth-stabilized cubic zirconia systems. In this case, the Zr-O coordination is further reduced to sixfold,[18] where minimal d-p mixing is expected.) The second feature labeled B in Fig. 9 is the splitting of the main peak. It becomes progressively more pronounced as the Y_2O_3 concentration increases. This tendency can be assessed more easily by inspecting the first derivative, where the splitting is now manifest as the separation between the zero crossings of a small peak marked as B' in Fig. 10. A similar splitting has been reported for Zr in Y_2O_3 (Ref. 22) and for rare-earth-stabilized cubic ZrO_2 systems.[18] Last, we note a third feature labeled C in Fig. 9. The intensity of this peak decreases with increasing Y concentration. Although peak C is probably also a structure-dependent feature, no interpretation will be attempted here in view of the complicated multiple-scattering processes that occur in this energy region.

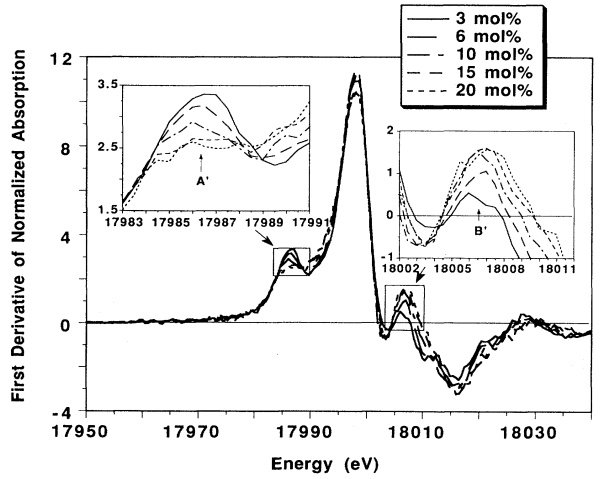

FIG. 10. First derivative of Zr XANES for Y-doped zirconia.

IV. DISCUSSION

A. Location of oxygen vacancies

A single charge-compensating oxygen vacancy is generated by every two substitutional Y atoms. There are three possibilities for the position of this vacancy, as shown in Fig. 11: (1) Both Y atoms are NN's to the oxygen vacancy, (2) only one Y atom is a NN to the oxygen vacancy, or (3) neither Y atom is a NN to the oxygen vacancy. Assuming oxygen has fourfold coordination, we can calculate the expected fractions of ZrO_8, ZrO_7, YO_8, and YO_7 polyhedra for each of these possibilities at different compositions. The results of these calculations are summarized in Table IV.

Previous attempts to distinguish between the models were based on comparing the coordination numbers[11,13,14,16] or the bond lengths.[15,17,18] Since the absolute value of N_{CN} can be in error by as much as 20%,[19] it is not a credible comparison for the present purpose. The tabulated ionic radii (Shannon[24]), which are deduced from compounds, are also questionable for solutes in solid solutions and must be calibrated judiciously. Since XANES features are sensitive to local geometry, we will use them and some calibrated data on the Y-O bond length in Zr-Y-Nb-O solid solutions to make our arguments for model (3). Additional evidence from EXAFS is also cited to support our argument.

The XANES feature A is sensitive to the symmetry of the Zr-O polyhedra. In monoclinic and orthorhombic zirconia, both with sevenfold coordination, no resolvable peak is observed at this energy.[4] In the other extreme, tetragonal zirconia has a prominent shoulder which we attributed to d-p mixing enhanced by the approximately dual tetrahedral local symmetry. Using the intensity of this feature as a measure of the fraction of Zr ions in the ZrO_8 structure (which splits into two tetrahedra), we can compare the relative population of ZrO_8 and ZrO_7 calculated in Table IV with the strength of this peak in Fig. 10. From such a comparison, we find that model (3)—i.e., neither Y atom is a NN of oxygen vacancy—is most consistent with the observed peak intensity variation. For

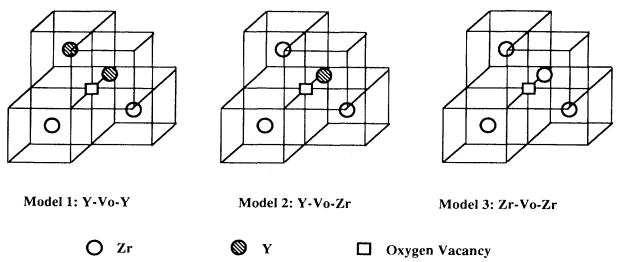

FIG. 11. Schematic illustration of three models for cation-oxygen vacancy (V_0) association.

TABLE IV. Calculated fractions of four types of oxygen polyhedra around Zr and Y for different models of cation-vacancy association.[a]

Composition (mol %)		Model (1) (Y-V_O-Y)			Model (2) (Y-V_O-Zr)				Model (3) (Zr-V_O-Zr)		
Y_2O_3	$YO_{1.5}$	YO_7	ZrO_8	ZrO_7	YO_8	YO_7	ZrO_8	ZrO_7	YO_8	ZrO_8	ZrO_7
3	5.8	5.8	88.4	5.8	2.9	2.9	85.5	8.7	5.8	82.6	11.6
6	11.3	11.3	77.4	11.3	5.7	5.7	71.6	17.0	11.3	66.1	22.6
10	18.2	18.2	63.6	18.2	9.1	9.1	54.5	27.3	18.2	45.4	36.4
15	26.1	26.1	47.8	26.1	13.1	13.1	34.6	39.2	26.1	21.7	52.2
20	33.3	33.3	33.4	33.3	16.7	16.7	16.6	50.0	33.3	0.0	66.7

[a]See Fig. 11 and text.

example, only model (3) correctly predicts a very low ZrO_8 concentration at 15 and 20 mol % Y_2O_3 to account for the very flat shoulder seen at these compositions. Model (1) predicts that at 20% Y_2O_3, and certainly at 15% Y_2O_3, at least one-half of Zr is still in eightfold coordination. If this were true, the shoulder should still be quite evident. Model (2) predicts that at 15% Y_2O_3, 47% of Zr is in eightfold coordination, while at 20% Y_2O_3, 25% of Zr is in eightfold coordination. Thus a major difference in the intensity of this feature should be evident between these compositions. In fact, Figs. 9 and 10 show essentially no shoulder for either composition, suggesting a very low ZrO_8 population in both cases.

We note that the Y-O distance is 2.33 Å in all of the samples that we analyzed. As reported elsewhere,[25] the Y-O bond length in ZrO_2-$YNbO_4$ solid solution is also about 2.33 Å. Since the latter contains no charge-compensating oxygen vacancies, according to the ionic conductivity studies of Choudhary and Subbarao[26] on isostructural ZrO_2-$YTaO_4$ solid solutions, the coordination of Y in ZrO_2-$YNbO_4$ is most certainly eightfold. The identical Y-O distance in these compounds then implies the same coordination for ZrO_2-Y_2O_3 solid solutions. This again argues for model (3). The Y-O bond distance obtained here is actually smaller than the Shannon distance for eightfold coordination (2.40 Å). Indeed, it would have corresponded to sevenfold coordination according to Shannon,[24] hence the basis of such a claim in some previous studies.[15,17,18] This difference, however, is due to a contraction of the oversized YO_8 and not a change in coordination number. For example, the oversized CeO_8 polyhedron in ZrO_2-CeO_2 solid solution is compressed to have a bond length of 2.30 Å which is smaller than that of CeO_2 (2.35 Å).[25,27] Thus a direct comparison with Shannon's table is very misleading for solute cations. Similar distances for eightfold-coordinated Y-O have also been found in $YNbO_4$ (2.32 Å) (Ref. 28) and $YTaO_4$ (2.35 Å).[29]

The structural model above has several important consequences. First, since Y does not have NN oxygen vacancies, it maintains eightfold coordination at all compositions, giving a constant Y-O distance. Second, the average Zr coordination number decreases from nearly 8 to 7 as Y_2O_3 concentration increases from 3 to 20 mol %. This is reflected in the very different Zr-O distances at the two compositions. The model can also explain the following unusual features related to the distortion of the EXAFS spectra of the solid solutions.

(a) Comparing Figs. 2 and 4, the amplitude for the Zr-cation shell is higher than that for the Y-cation shell at 3 mol % Y_2O_3, but the opposite is true at 20 mol % Y_2O_3. This is probably because MO_7 polyhedra are not regular features of the fluorite structure. Thus the change from ZrO_8 to ZrO_7 causes much distortion of the Zr-centered cation network, whereas maintaining YO_8 at all compositions is able to minimize the distortion.

(b) At room temperature only the inner Zr-O subshell ($Zr\text{-}O_I$) for ZrO_8 structures is seen. As the Y_2O_3 concentration increases, ZrO_8 is replaced by ZrO_7 which has a longer bond distance than $Zr\text{-}O_I$. Thus the apparent Zr-O bond length increases. The outer shell ($Zr\text{-}O_{II}$), nevertheless, contributes a relatively broad background to EXAFS. Thus, as the ZrO_8 population decreases, i.e., at higher Y_2O_3 concentration, the σ^2 for Zr-O shell decreases.

(c) The Zr-cation network distortion at high Y concentration has been shown to involve a cation displacement of 0.18 Å along the ⟨111⟩ direction.[5] We showed that this can account for the observed Debye-Waller factor for the ZrO_7 structure at 20 mol % Y_2O_3.[4] This distortion of the cation network is noncentrosymmetric and is probably responsible for the apparent contraction of the bond distance when the EXAFS data are analyzed by assuming a Gaussian dispersion.

B. Comparison with VCA

Finally, we compare the EXAFS data with the XRD lattice parameter data given in Table I. It can be seen that the lattice parameter increases slowly over the composition range investigated, in contrast to the approximately constant (or perhaps slightly *decreasing*) cation-cation distance seen by EXAFS. The 3.62 Å EXAFS distance corresponds to a fluorite lattice parameter of 5.12 Å. This is close to the weighted average of tetragonal lattice parameters at 3 mol % Y_2O_3 (5.1308 Å) but substantially smaller than the cubic lattice parameter at 20 mol % Y_2O_3 (5.1748 Å). Similarly, the weighted average of the EXAFS cation-O distances is smaller than the calculated XRD distance inferred for an ideal fluorite-type structure (2.18 vs 2.23 Å at 10 mol % Y_2O_3 and 2.21 vs 2.24 Å at 20 mol % Y_2O_3). In other words, our EXAFS results for both cation-oxygen distance and cation-cation distance depart from those deduced from the convention-

al VCA. (It states that all atoms occupy the average lattice positions defined by the x-ray lattice constant.) These discrepancies can best be understood if we accept the picture that fully stabilized cubic zirconia is only "cubic" in an average sense over a large distance compared to the cation spacing and that the actual cation positions, especially those of Zr, are significantly displaced from the ideal fluorite lattice points to accommodate the severe distortion necessitated by ZrO_7 polyhedra. The observed lattice expansion with increasing Y concentration is then not due to the increasing distance from center to center between cation-oxygen polyhedra, but rather due to the increasingly inefficient (i.e., less compact) packing of the polyhedra.

V. CONCLUSIONS

(1) Oxygen vacancies, caused by Y doping in zirconia, are preferentially located as nearest neighbors of Zr, leaving eightfold coordination to Y.

(2) The bond distance of YO_8 polyhedra (2.33 Å) and the Y-cation distance (3.62 Å) are nearly the same in both tetragonal and cubic solid solutions. Thus the dopant cation can maintain substantially the same local structure in different host polymorphs.

(3) The distortion of both Zr and Y local environments generally increases with alloying. In particular, the Zr-cation shell in cubic zirconia is most severely distorted. This is required to accommodate ZrO_7 polyhedra which are not regular features of the fluorite-type structure.

(4) The Zr–Y-O and Zr–Y-cation distances obtained from EXAFS for cubic zirconia depart from the estimated values using the XRD lattice parameter based on the virtual-crystal approximation. Thus the long-range, fluorite-like order implied by global cubic symmetry is not manifested in the local atomic environment.

ACKNOWLEDGMENTS

This research is supported by the National Science Foundation Grant No. DMR-9119598. The NSLS and SSRL facilities are operated by the U.S. Department of Energy with additional support from the U.S. National Institute of Health.

[1]J. Lefèvre, Ann. Chim. **8**, 117 (1963).
[2]T. S. Sheu, T. Y. Tien, and I-W. Chen, J. Am. Ceram. Soc. **75**, 1108 (1992).
[3]M. Yoshimura, Bull. Am. Ceram. Soc. **67**, 1950 (1988).
[4]P. Li, I-W. Chen, and J. E. Penner-Hahn, preceding paper, Phys. Rev. B **48**, 10 063 (1993).
[5]D. Steel and B. E. F. Fender, J. Phys. C **7**, 1 (1974).
[6]M. Morinaga, J. B. Cohen, and J. Faber, Jr., Acta Crystallogr. A **35**, 789 (1979).
[7]M. Morinaga, J. B. Cohen, and J. Faber, Jr., Acta Crystallogr. A **36**, 520 (1980).
[8]J. Dexpert-Ghys, M. Faucher, and P. Caro, J. Solid State Chem. **54**, 179 (1984).
[9]J. G. Allpress and H. J. Rossell, J. Solid State Chem. **15**, 68 (1975).
[10]A. Dwivedi and A. N. Cormack, Philos. Mag. A **61**, 1 (1990).
[11]A. I. Goldman, E. Canova, Y. H. Kao, W. L. Roth, and R. Wang, in *EXAFS and Near Edge Structure III,* edited by K. O. Hodgson, B. Hedman, and J. E. Penner-Hahn (Springer-Verlag, New York, 1984), pp. 442–444.
[12]C. R. A. Catlow, A. V. Chadwick, G. N. Greaves, and L. M. Moroney, J. Am. Ceram. Soc. **69**, 272 (1986).
[13]M. H. Tuilier, J. Dexpert-Ghys, H. Dexpert, and P. Lagarde, J. Solid State Chem. **69**, 153 (1987).
[14]B. W. Veal, A. G. Mckale, A. P. Paulikas, S. J. Rothman, and L. J. Nowicki, Physica B **150**, 234 (1988).
[15]H. Morikawa, Y. Shimizugawa, F. Marumo, T. Harasawa, H. Ikawa, K. Tohji, and Y. Udagawa, J. Jpn. Ceram. Soc. **96**, 253 (1988).
[16]Z. J. Shen, T. K. Li, K. Q. Lu, and Y. Q. Zhao, J. Chin. Silic. Soc. **16**, 270 (1988).
[17]E. Zschech, G. Auerswald, E. D. Klinkenberg, and B. N. Novgorodov, Nucl. Instrum. Methods Phys. Rev. A **308**, 255 (1991).
[18]D. Komyoji, A. Yoshiasa, T. Moriga, S. Emura, F. Kanamaru, and K. Koto, Solid State Ion. **50**, 291 (1992).
[19]B. K. Teo, *EXAFS: Basic Principles and Data Analysis* (Springer-Verlag, New York, 1986).
[20]V. S. Stubican, in *Science and Technology of Zirconia III,* edited by S. Somiya, N. Yamamoto, and H. Hanagida, Advances in Ceramics Vol. 24 (The American Ceramic Society, Westerville, OH, 1988), pp. 71–82.
[21]J. J. Rehr, J. Mustre de Leon, S. I. Zabinsky, and R. C. Albers, J. Am. Chem. Soc. **113**, 5135 (1990).
[22]N. Thromat, C. Noguera, M. Gautier, F. Joelet, and J. P. Duraud, Phys. Rev. B **44**, 7904 (1991).
[23]F. Jollet, C. Noguera, N. Thromat, M. Gautier, and J. P. Duraud, Phys. Rev. B **42**, 7587 (1990).
[24]R. D. Shannon, Acta Crystallogr. A **32**, 751 (1976).
[25]P. Li, I-W. Chen, and J. E. Penner-Hahn, J. Am. Ceram. Soc. (to be published).
[26]C. B. Choudhary and E. C. Subbarao, in *Fast Ion Transport in Solids,* edited by P. Vashishta, J. N. Mundy, and G. K. Shenoy (Elsevier, New York, 1979), pp. 665–668.
[27]Y. Shimizugawa, H. Morikawa, F. Marumo, A. Nakajima, K. Urabe, and M. Normura, J. Jpn. Ceram. Soc. **95**, 1131 (1987).
[28]A. I. Komkov, Kristallografiya **4**, 836 (1959).
[29]L. H. Brixner and H. Y. Chen, J. Electrochem. Soc. **130**, 2435 (1983).